Applied Catalysis B: Environmental 168-169 (2015) 423–428

Contents lists available at ScienceDirect

Applied Catalysis B: Environmental

journal homepage: www.elsevier.com/locate/apcatb

Highly efficient hydrogen generation from formic acid-sodium formate over monodisperse AgPd nanoparticles at room temperature

Lan Yang[a], Xing Hua[a], Jun Su[c], Wei Luo[a,b,*], Shengli Chen[a], Gongzhen Cheng[a,**]

[a] College of Chemistry and Molecular Sciences, Wuhan University, Wuhan, Hubei 430072, PR China
[b] Suzhou Institute of Wuhan University, Jiangsu, Suzhou 215123, PR China
[c] Wuhan National Laboratory for Optoelectronics, Huazhong University of Science and Technology, Wuhan, Hubei 430074, PR China

ARTICLE INFO

Article history:
Received 20 September 2014
Received in revised form
26 December 2014
Accepted 5 January 2015
Available online 6 January 2015

Keywords:
Silver
Palladium
Graphene
Formic acid
Hydrogen storage

ABSTRACT

Monodisperse AgPd alloy nanoparticles are synthesized by co-reduction of silver nitrate and palladium acetylacetonate in 1-octadecene and oleic acid using tert-butylamine borane as the reducing agent at 60 °C. Thanks to the narrow size distribution of the AgPd alloy NPs and the synergistic effect with graphene, the as-synthesized $Ag_{74}Pd_{26}$/graphene exerts nearly 100% hydrogen selectivity and exceedingly high catalytic activity toward hydrogen generation from formic acid at room temperature, with the turnover frequency value of 572 h^{-1}.

1. Introduction

The safe and efficient storage of hydrogen is essential for the development of a hydrogen-based energy infrastructure. For the last few decades, there has been rapidly growing interest in searching for suitable hydrogen storage materials, including metal hydrides [1], sorbent materials [2], and chemical hydrides [3]. Among them, the liquid-phase hydrogen storage materials, which are easy to handle and transport (using the existing liquid-based fuel distribution infrastructure), without the involvement of any solid byproduct, have been considered more advantageous over traditional solid-phase hydrogen storage materials [4]. Formic acid (FA), a major product of biomass processing, has attracted considerable attention as a safe and convenient hydrogen storage material due to its high hydrogen content, nontoxicity, liquid at room temperature and easy recharging ability [5]. Hydrogen stored in FA can be released through a catalytic dehydrogenation way Eq. (1). However, from a perspective of hydrogen storage, the undesirable dehydrogenation way Eq. (2) should be avoided because CO is toxic to the fuel cell catalysts [6].

$$HCOOH(l) \rightarrow H_2(g) + CO_2(g) \Delta G_{298\,K} = -35.0\,KJ\,mol^{-1} \quad (1)$$

$$HCOOH(l) \rightarrow H_2O(l) + CO(g) \Delta G_{298\,K} = -14.9\,KJ\,mol^{-1} \quad (2)$$

To this end, a number of noble metals and their alloys based nanocatalysts have been recently developed [7], however, catalysts possessing prominent activity and selectivity at room temperature are still few [8].

Recently, bimetallic AgPd alloy nanoparticles (NPs) have been found to be efficient catalysts toward dehydrogenation of FA. For example, Zhou et al. reported CeO_2 supported AgPd NPs, with an initial turnover frequency (TOF) of 68.5 h^{-1} toward dehydrogenation of FA-sodium formate (SF) mixture at 92 °C [9a]. Very recently, we have reported AgPd NPs immobilized into the metal-organic frameworks (MIL-101), which exhibit high catalytic activity for the conversion of FA to high-quality of hydrogen at 80 °C with TOF of 848 h^{-1} from FA-SF mixture [9b]. Yan and co-workers reported a in situ synthesis of rGO supported AgPd catalyst with TOF of 105.2 h^{-1} for the hydrogen liberation from FA-SF mixture at room temperature [9c]. Sun and co-workers synthesized monodisperse 2.2 nm AgPd NPs by co-reduction of Ag, Pd precursors in oleylamine (OAm), oleic acid (OA) and 1-octadecene (ODE) at relatively high temperature 180 °C, which could afford a TOF value of 382 h^{-1} at 50 °C for dehydrogenation of FA after loading onto carbon [9d].

* Corresponding author at: College of Chemistry and Molecular Sciences, Wuhan University, Wuhan, Hubei 430072, PR China. Tel.: +86 2787467716.
** Corresponding author.
E-mail addresses: wluo@whu.edu.cn (W. Luo), gzcheng@whu.edu.cn (G. Cheng).

http://dx.doi.org/10.1016/j.apcatb.2015.01.003
0926-3373/

Thus, the development of high-performance catalysts for the dehydrogenation of FA at room temperature is highly desirable for practical application.

In light of the previous work about the effects of morphology of metal NPs and supported materials, the ultrafine metal NPs with a narrow size distribution and high dispersion may be conductive to their catalytic performance toward dehydrogenation of FA. Herein, we report a facile synthesis of monodisperse AgPd NPs and their catalytic activity toward hydrogenation generation from FA-SF solution at room temperature. Graphene, a single-layer of sp^2 carbon lattices, with many advantages such as high specific surface area [10a], thermal and chemical stability [10b], outstanding charge carrier mobility [10c], and superior electrical conductivity [10d], etc., was chosen as the substrate to anchor AgPd NPs with good dispersion. As expected, the resultant $Ag_{74}Pd_{26}$/graphene NPs exert exceedingly high catalytic activity and nearly 100% hydrogen selectivity toward dehydrogenation of FA at room temperature.

2. Experiments

2.1. Materials

Silver nitrate ($AgNO_3$, AR), palladium acetylacetonate ($Pd(acac)_2$, >98%, Wuhan Greatwall Chemical Co., Ltd.), tert-butylamine borane ($BH_3{\cdot}C_4H_{11}N$, TBB, >95%, TCI Shanghai Co., Ltd.), triethylamine borane ($BH_3{\cdot}C_6H_{15}N$, TEB, >90.0%, TCI Shanghai Co., Ltd.), sodium borohydride ($NaBH_4$, Sinopharm Chemical Reagent Co., Ltd., ≥96%), methylamine hydrochloride ($CH_3NH_2{\cdot}HCl$, Sinopharm Chemical Reagent Co., Ltd., ≥96%), tetrahydrofuran (C_4H_8O, Sinopharm Chemical Reagent Co., Ltd., ≥99%), dimethyl ether anhydrous ($C_4H_{10}O$, Sinopharm Chemical Reagent Co., Ltd., ≥99.7%), Ketjen carbon (Sinopharm Chemical Reagent Co., Ltd.), graphite power (≥99.85%, Sinopharm Chemical Reagent Co., Ltd.), potassium permanganate ($KMnO_4$, ≥99.5%, Shanghai Chemic Co., Ltd.), phosphoric acid (H_3PO_4, AR, Sinopharm Chemical Reagent Co., Ltd.), sulfuric acid (H_2SO_4, 95–98%, Sinopharm Chemical Reagent Co., Ltd.), hydrogen peroxide (H_2O_2, ≥30%, Sinopharm Chemical Reagent Co., Ltd.), hydrazine hydrate ($N_2H_4{\cdot}H_2O$, ≥85%), 1-octadecene (ODE, >90%, Aladdin Industrial Corporation), oleic acid ($C_{18}H_{34}O_2$, AR, Sinopharm Chemical Reagent Co., Ltd.). All chemicals were used as obtained. We use ordinary distilled water as the reaction solvent.

2.2. Preparation of graphite oxide (GO) and graphene

The synthesis method of GO was synthesized according to the literature [11a]. In an improved synthesis of graphite oxide, a 9:1 mixture of concentrated H_2SO_4/H_3PO_4 (360:40 mL) was added to a mixture of graphite flakes (3.0 g) and $KMnO_4$ (18.0 g). The reaction was then heated to 50 °C and stirred for 12 h. The reaction was cooled to room temperature and poured onto ice (~400 mL) with 30% H_2O_2 (3 mL). The addition of 2 mL of excess H_2O_2 was followed until observation of a permanent yellow color, which indicating the complete oxidation of graphite. The resultant solution was centrifuged to obtain the product. The product was washed by deionized water, 30% diluted hydrochloric acid and absolute ethyl alcohol for many times and dried under vacuum at 25 °C. The synthesis method of graphene was synthesized according to the literature [11b]. 500 mg of dried GO was dissolved in 500 mL of water and the mixture was sonicated to exfoliate GO in water until no visible particle was observed in the solution. Then, 5.0 mL of hydrazine hydrate was added into the aqueous dispersion of GO. Then, the resultant solution was connected to reflux system and refluxed at 100 °C for 18 h. Due to the reduction of graphite oxide, the floating black particles were observed at the end of the reflux process indicating the formation of graphene nanosheets. Finally, the graphene nanosheets were filtered by suction filtration and washed three times with water and ethanol, respectively. The powder samples were dried under vacuum.

2.3. Preparation of methylamine borane ($CH_3NH_2BH_3$, MeAB)

MeAB was synthesized by the method reported in the literature [12]. Sodium borohydride (3.783 g, 0.1 mol) and methylamine hydrochloride (6.752 g, 0.1 mol) were added to a 500 mL two-neck round-bottom flask with a neck connected to a condenser. THF (200 mL) was transferred into the flask with vigorously stirring. The reaction was carried out at room temperature under nitrogen atmosphere. After 12 h, the resultant solution was filtered and the filtrate was concentrated under vacuum at room temperature. The product was purified by ether.

2.4. Synthesis of AgPd nanoparticles (NPs)

Under a gentle nitrogen flow, 16.9 mg of silver (I) nitrate ($AgNO_3$, 0.1 mmol) and 30.4 mg of palladium (II) acetylacetonate ($Pd(acac)_2$, 0.1 mmol) were magnetically stirred in 5 mL 1-octadecene (ODE) and 2.5 mL oleic acid (OA). The mixture was heated to 60 °C to generate a homogeneous solution. And the mixture kept at this temperature for 30 min to remove oxygen. 1 mmol TBB, TEB, MeAB was quickly added into the solution, respectively. A visible color change from colorless to a brown-black was observed. The temperature was kept at 60 °C for 30 min. Once the reaction solution was cooled down to room temperature, the NPs were separated by adding ethanol and centrifugation (8500 rpm, 5 min).

2.5. Synthesis of AgPd/graphene catalysts

80 mg of graphene and 20 mg of AgPd NPs were dispersed in 10 mL of hexane. The mixture was sonicated for 10 min, and then stirred 12 h under a nitrogen flow. The NPs were separated by adding ethanol and centrifugation (8500 rpm, 5 min). Next, the AgPd/graphene NPs were suspended in 30 mL of acetic acid and the suspension was heated at 70 °C overnight. 30 mL of ethanol was added and the mixture was centrifuged at 8500 rpm for 5 minutes. This ethanol washing procedure was repeated three times. The AgPd/graphene NPs were recovered and dried under vacuum.

2.6. H_2 generation from FA aqueous solution

Typically, the as-prepared AgPd/graphene (60 mg) was kept in a two-necked round-bottom flask. One neck was connected to a gas burette, and the other was connected to a pressure-equalization funnel to introduce FA/SF aqueous solution ($c_{FA} + c_{SF} = 1.0$ M, $c_{FA}/c_{SF} = 9{:}1$, 2 mL). The catalytic reaction was begun once the FA/FS solution was added into the flask with magnetic stirring. The evolution of gas was monitored by the gas burette. The reaction was carried out at 298 K under ambient atmosphere.

2.7. CO stripping experiment

Electrochemical measurements were performed with a three electrode configuration. The electrolyte was 0.1 M $HClO_4$ aqueous solution. The working electrodes were the commonly used thin-film RDE made by coating the catalyst samples as a thin film onto a GC RDE substrate (diameter: 5 mm) with Nafion as the binding agent. Briefly, 2.5 mg catalyst were dispersed in 1 mL Nafion/isopropyl alcohol solution (1 mL 5 wt% Nafion mixed with 49 mL isopropyl alcohol) to form the catalyst ink and 6 μL ink was pipetted onto the GC RDE. The counter electrode was a Pt foil. The reference electrode was a saturated calomel electrode (SCE).

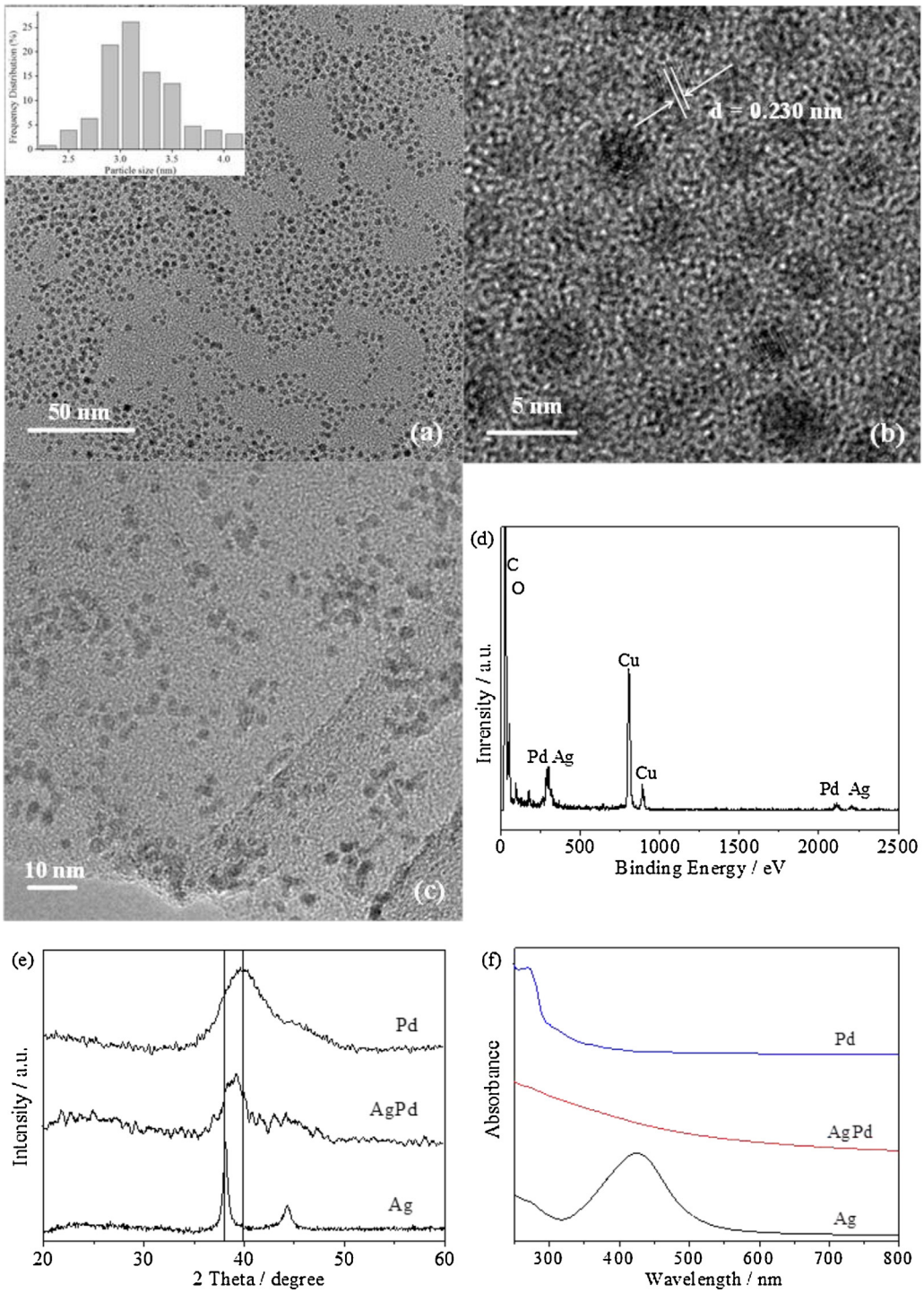

Fig. 1. (a) TEM image of the 3.0 ± 0.2 nm nm $Ag_{74}Pd_{26}$ NPs, and inset: particle size of $Ag_{74}Pd_{26}$ NPs. (b) HRTEM image of the $Ag_{74}Pd_{26}$ NPs. (c) TEM image of the graphene-supported $Ag_{74}Pd_{26}$ NPs after treatment with acetic acid. (d) EDX of $Ag_{74}Pd_{26}$ NPs reduced by BTB. (e) XRD patterns of the Ag, $Ag_{74}Pd_{26}$, and Pd NPs (the vertical line left and right denote standard (1 1 1) peak positions of bulk Ag and Pd, respectively). (f) UV–vis spectra of the Ag, $Ag_{74}Pd_{26}$, and Pd NPs.

For CO stripping voltammetry, the $HClO_4$ (0.1 M) solution was first purged with CO gas for ca. 30 min. while keeping the electrode potential constantly at −0.178 V; Ar gas was then bubbled into solution for 30 min. under the same potential to remove the CO in the solution, following which a potential cycling of $-0.178\,V \rightarrow 0.86\,V \rightarrow -0.3\,V \rightarrow 0.86\,V \rightarrow -0.3\,V$ was performed with a potential sweeping rate of 20 mV/s and the corresponding voltammetric curves were recorded.

2.8. Characterization

TEM images were obtained using a FEI Tecnai G20 TEM/Titan G260–300 Probe Cs Corrector HRSTEM instrument operating at 200 kV. Powder X-ray diffraction (XRD) patterns were measured by a Bruker D8-Advance X-ray diffractometer using Cu Ka radiation source ($\lambda = 0.154178$ nm) with a velocity of $6^\circ\,min^{-1}$. FTIR spectra were collected at room temperature by using a Thermo

FTIR-iS10 instrument using KBr discs in the 400–4000 cm^{-1} region. Raman spectra were carried out using a confocal Raman microscope (Renishaw, RM-1000) at 514.5 nm excitation. X-ray photoelectron spectroscopy (XPS) measurement was performed with a Kratos XSAM 800 spectrophtometer. Detailed analyses for CO_2, H_2 and CO were performed on GC-2020 with thermal conductivity detector (TCD) and flame ionization detector (FID)-Methanator (detection limit: ~10 ppm to CO). UV–vis absorption spectra were recorded on TU-1810 UV–vis spectrophotometer. The inductively coupled plasma-atomic emission spectroscopy (ICP-AES) was performed on IRIS Intrepid II XSP (Thermo Fisher Scientific, USA). The electrochemical measurements were performed on CHI660A electrochemical workstation (ShanghaiChenhua Co., China).

3. Results and discussion

The monodisperse AgPd alloy NPs were prepared by co-reduction of silver nitrate ($AgNO_3$) and palladium acetylacetonate ($Pd(acac)_2$) in 1-octadecene (ODE) and oleic acid (OA) using tert-butylamine borane (TBB) as the reducing agent at 60 °C. The composition of the AgPd NPs was controlled by varying the initial molar ratio of $AgNO_3$ and $Pd(acac)_2$, and further analyzed by inductively coupled plasma-atomic emission spectroscopy (ICP-AES) (Table S1). The microstructures of the as-synthesized AgPd NPs with different compositions were characterized by transmission electron microscopy (TEM). As shown in Fig. 1a and Fig. S1, the AgPd NPs have a narrow size distribution with a mean particle size of 3.0 ± 0.2 nm. A representative high-resolution TEM (HRTEM) image of $Ag_{74}Pd_{26}$ NPs in Fig. 1b shows the d-spacing of 0.23 nm, which is between the (1 1 1) lattice spacing of face-centered cubic (fcc) Ag (0.235 nm) and Pd (0.224 nm), suggesting that AgPd is formed as an alloy structure. The energy dispersive X-ray (EDX) spectra (Fig. 1d) further confirm the coexistence of Ag and Pd. Fig. 1e shows the powder X-ray diffraction (XRD) patterns of the as-synthesized Ag, Pd and $Ag_{74}Pd_{26}$ NPs. The well-defined diffraction peak of $Ag_{74}Pd_{26}$ NPs is between the peaks of Ag and Pd NPs, further indicating that AgPd is formed as an alloy and not as a core-shell structure. Furthermore, the formation of alloy structure was confirmed by UV–vis spectra. As shown in Fig. 1f, Ag NPs have strong surface plasmon resonance (SPR) absorption at 427 nm, and Pd NPs have no SPR absorption, however, AgPd NPs exhibit almost no SPR absorption. This result indicates that alloying Pd with Ag could affect the SPR absorption of Ag drastically. The FTIR spectra of GO and AgPd/graphene were showed in Fig. S2. It can be seen clearly that the disappearance of C=O peak at 1736 cm^{-1}, C—OH peak at 1227 cm^{-1} and the C—O peak at 1057 cm^{-1} of GO, indicating GO is reduced to graphene. In the Raman spectroscopy (Fig. S3), the GO and graphene supported AgPd NPs exhibit two peaks centered at 1331 and 1590 cm^{-1}, corresponding to the D and G bands of the carbon products, respectively. The intensity ratio of the D to G band (I_D/I_G) is generally accepted to reflect the degree of graphitization of carbonaceous materials and defect density. After reduced by hydrazine hydrate, the I_D/I_G of GO is increased from 1.6 to 2.1, which further confirms the reduction of GO. X-ray photoelectron spectroscopy (XPS) measurements are performed to determine the composition and chemical state of the as-synthesized AgPd NPs. As shown in Fig. S4a–b shows the XPS of the GO, and AgPd/graphene catalysts. Compared with the peaks of GO (Fig. S4a), the intensities of the oxygen containing functional groups (such as —C—O, —C=O, —COO) in AgPd/graphene (Fig. S2b) decrease significantly, which also reveal the reduction of GO. Figure S4c shows that the $3d^{5/2}$ and $3d^{3/2}$ peaks of Ag0 appear at 374.0 and 367.5 eV with no obvious peak of Ag^+ was observed [13], while in Fig. S4d, the $3d^{5/2}$ and $3d^{3/2}$ peaks of Pd° appear at 335.7 and 341.0 eV [14–16], with no obvious peak of Pd^{2+} was observed, indicating the co-existence of both metals.

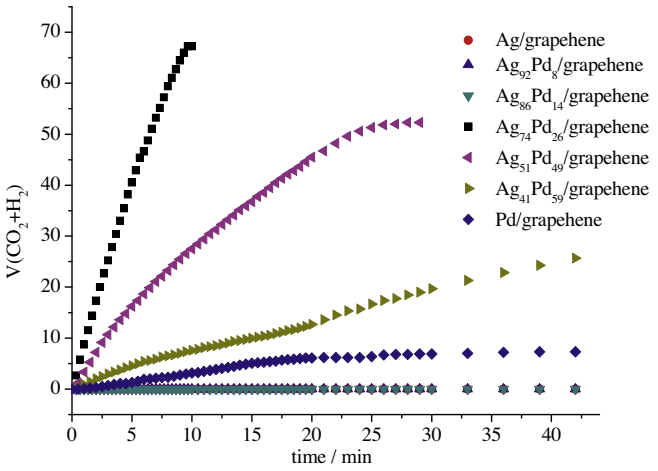

Fig. 2. The plots of generated gas ($CO_2 + H_2$) versus time from FA/SF aqueous solution ($c_{FA} + c_{SF}$ = 1.0 M, c_{FA}/c_{SF} = 9:1, 2 mL) in the presence of different catalysts: Ag/graphene, $Ag_{92}Pd_8$/graphene, $Ag_{86}Pd_{14}$/graphene, $Ag_{74}Pd_{26}$/graphene, $Ag_{51}Pd_{49}$/graphene, $Ag_{41}Pd_{59}$/graphene, and Pd/graphene at room temperature.

To study their catalytic performance, the as-synthesized AgPd NPs were deposited on graphene and further treated with acetic acid at 70 °C overnight [9d]. TEM image indicated the AgPd NPs were well dispersed on graphene as shown in Fig. 1c. In addition, the ICP-AES analysis confirmed the composition of the AgPd NPs was not changed. The catalytic activities of AgPd/graphene NPs with different compositions, together with Ag/graphene and Pd/graphene for hydrogen generation from FA at room temperature are presented in Fig. 2. We can see that neither Ag nor Pd is active toward dehydrogenation of FA. Among all the bimetallic AgPd/graphene NPs investigated, $Ag_{74}Pd_{26}$/graphene exhibits the highest catalytic activity with the turnover frequency (TOF) value of 572 h^{-1} at room temperature, which is higher than most of the previously reported values (Table S2) [17,18]. In addition, we have tested the catalytic activity of AgPd NPs without support and AgPd NPs supported on Ketjen carbon toward dehydrogenation of FA, as shown in Fig. S5, they are both inferior to that of AgPd NPs supported on graphene, highlighting the positive effect of utilization of graphene as a two-dimensional support in facilitating the electron transfer and mass transport [19]. The composition of the gas

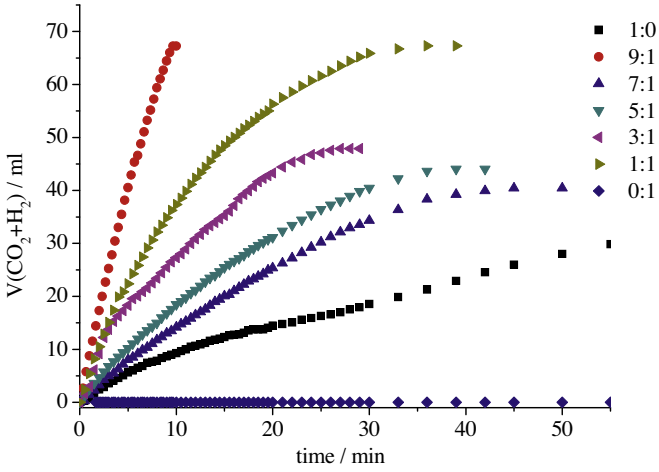

Fig. 3. The plots of generated gas ($CO_2 + H_2$) versus time from FA/SF aqueous solution with different molar ratio of FA and SF catalyzed by $Ag_{74}Pd_{26}$/graphene at room temperature.

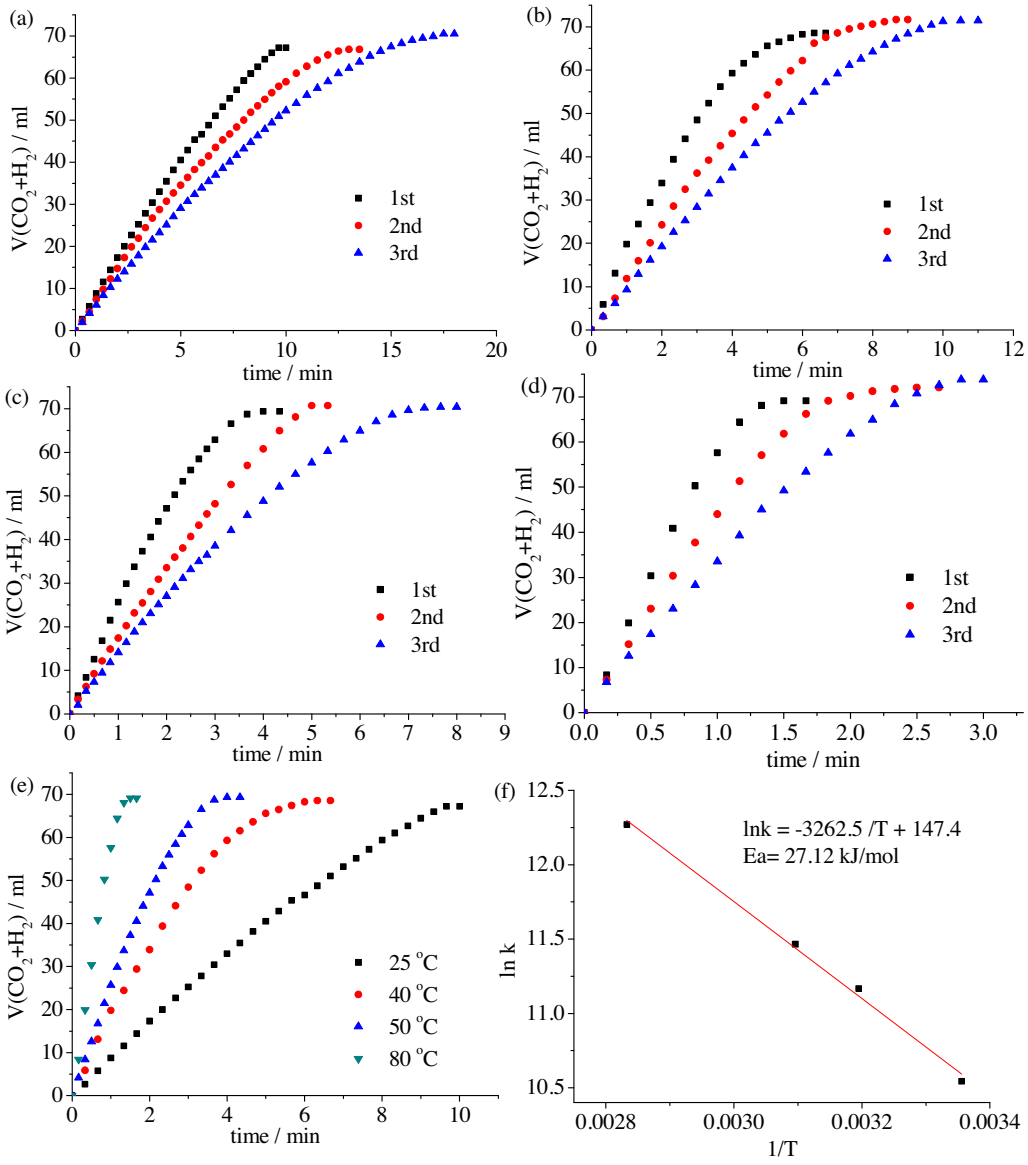

Fig. 4. (a)–(d) The plots of generated gas ($CO_2 + H_2$) versus time from FA/SF aqueous solution ($c_{FA} + c_{SF}$ = 1.0 M, c_{FA}/c_{SF} = 9:1, 2 mL) catalyzed by $Ag_{74}Pd_{26}$/graphene from 1st to 3rd cycles at 25 °C, 40 °C, 50 °C, and 80 °C, respectively. (e) The plots of generated gas ($CO_2 + H_2$) versus time from FA/SF aqueous solution catalyzed by $Ag_{74}Pd_{26}$/graphene at four different temperatures. (f) Arrhenius plot obtained from the data of Fig. 4(e).

was further analyzed by gas chromatography (GC). As shown in Fig. S6 and S7, only the mixture of H_2 and CO_2 but no CO were detected, indicating the excellent H_2 selectivity for formic acid dehydrogenation by the as-synthesized AgPd/graphene catalyst. Fig. S8 shows cyclic voltammograms curves for Pd/graphene and AgPd/graphene in $HClO_4$ (0.1 M) solution. Hydrogen ad-/desorption peaks occurred for the Pd/graphene and AgPd/graphene catalysts below 0.05 V. Furthermore, the CO stripping voltammetry is used as a useful probe to reflect the anti-poisoning ability of noble metal surface toward CO. The AgPd/graphene catalyst exhibits more negative onset potential (0.49 V for AgPd versus 0.54 V for Pd) and lower voltammetric charge for CO oxidation than those for the Pd/graphene catalyst, which indicates that the AgPd/graphene catalyst is more capable of anti-poisoning to CO, probably due to the synergistic effect of AgPd alloy. [20,21] It is known that the molar ratio of FA/SF has a great effect on the catalytic activity of nanocatalysts. We studied the hydrogen generation from FA/SF solution with different FA/SF molar ratios over $Ag_{74}Pd_{26}$/graphene at 25 °C to obtain the best molar ratio of FA and SF in our system. From Fig. 3, we can see that without FA, no gas can be generated over the as-synthesized catalyst from SF, however, when the molar ratio of FA/SF is 9:1, the catalyst exhibits highest catalytic activity.

It has been reported that amine borane complexes are normally used as reducing agents for the size-controlled synthesis of metal nanocrystallites. [22–24] We found that the use of TBB is essential for synthesis of monodisperse AgPd NPs and enhancement of their catalytic activities. When TBB was replaced by other amine boranes with stronger reducing ability such as triethylamine borane (TEB) or methylamine borane (MeAB), it is difficult to obtain NPs with a narrow size distribution (Fig. S9). As a result, their catalytic activities are both inferior to that of AgPd NPs reduced by TBB as sown in Figure S10.

In addition, the reusability of the $Ag_{74}Pd_{26}$/graphene catalyst was examined by successively adding the same amount of FA after the completion of the previous run at different temperatures (Fig. 4a–d). The results showed that there is slight decrease in catalytic activity and no change in the hydrogen selectivity after the third run. The TEM of AgPd/graphene catalyst after three cycles

are shown in Fig. S11, the AgPd NPs were well dispersed on the graphene without no obvious agglomeration. However, the particle size was increased significantly, which may be the reason for the decrease in their catalytic activity. Further work about enhancement of the recyclability of the AgPd/graphene catalyst for dehydrogenation of FA is still underway. The Arrhenius plot of ln k versus 1/T for the catalyst is plotted Fig. 4f, from which the apparent activation energy (Ea) was determined to be approximately 27.12 kJ mol^{-1}, which is lower than most of reported values.

4. Conclusion

In summary, we have present a facile approach for the synthesis of monodisperse AgPd alloy NPs by tert-butylamine borane reduction of silver nitrate and palladium acetylacetonate in 1-octadecene and oleic acid at relatively low temperature. The alloy NPs were deposited on graphene and tested for their catalytic dehydrogenation of FA at room temperature. Among all the catalysts tested, $Ag_{74}Pd_{26}$/graphene exhibits a marked superiority over its monometallic and bimetallic counterparts with different ratios, indicating the strong molecular-scale synergy of Ag-Pd alloy. Thanks to the narrow size distribution of the AgPd NPs and the synergistic effect with graphene, the as-synthesized $Ag_{74}Pd_{26}$/graphene exerts nearly 100% hydrogen selectivity and exceedingly high catalytic activity, with initial TOF of 572 h^{-1}. This remarkable improvement of the catalytic performance by the controlled synthesis of narrow size distribution of alloy NPs and the utilization of graphene as a powerful support is believed to strongly promote the practical application of formic acid for chemical hydrogen storage in the fuel-cell hydrogen economy.

Acknowledgements

This work was financially supported by the National Natural Science Foundation of China (21201134), the Natural Science Foundation of Jiangsu Province (BK20130370), the Natural Science Foundation of Hubei Province (2013CFB288), the Creative Research Groups of Hubei Province (2014CFA007) and Large-scale Instrument and Equipment Sharing Foundation of Wuhan University.

Appendix A. Supplementary data

Supplementary data associated with this article can be found, in the online version, at http://dx.doi.org/10.1016/j.apcatb.2015.01.003.

References

[1] J. Graetz, Chem. Soc. Rev. 38 (2009) 73–82.
[2] M.P. Suh, H.J. Park, T.K. Prasad, D.W. Lim, Chem. Rev. 112 (2012) 782–835.
[3] A. Staubitz, A.P.M. Robertson, I. Manners, Chem. Rev. 110 (2010) 4079–4124.
[4] W. Luo, P.G. Campbell, L.N. Zakharov, S.Y. Liu, J. Am. Chem. Soc. 133 (2011) 19326–19329.
[5] M. Yadav, Q. Xu, Energy Environ. Sci. 5 (2012) 9698–9725.
[6] M. Yadav, T. Akita, N. Tsumori, Q. Xu, J. Mater. Chem. 22 (2012) 12582–12586.
[7] (a) K. Tedsree, T. Li, S. Jones, C.W.A. Chan, K.M.K. Yu, P.A.J. Bagot, E.A. Marquis, G.D.W. Smith, S.C.E. Tsang, Nature Nanotech. 6 (2011) 302–307.
[8] Z.L. Wang, J.M. Yan, H.L. Wang, Y. Ping, Q. Jiang, Sci. Rep. 2 (598) (2012) 1–6.
[9] (a) X.C. Zhou, Y.J. Huang, W. Xing, C.P. Liu, J.H. Liao, T.H. Lu, Chem. Commun. (2008) 3540–3542.
[10] (a) S. Garaj, W. Hubbard, A. Reina, J. Kong, D. Branton, J.A. Golovchenko, Nature 467 (2010) 190–194.
[11] (a) D.C. Marcano, D.V. Kosynkin, J.M. Berlin, A. Sinitskii, Z.Z. Sun, A. Slesarev, L.B. Alemany, W. Lu, J.M. Tour, ACS Nano 4 (2010) 4806–4814.
[12] Z.X. Yang, F.Y. Cheng, Z.L. Tao, J. Liang, J. Chen, Int. J. Hydrogen Energy 37 (2012) 7638–7644.
[13] L. Yang, J. Su, X.Y. Meng, W. Luo, G.Z. Cheng, J. Mater. Chem. A 1 (2013) 10016–10023.
[14] H.M. Dai, J. Su, K. Hu, W. Luo, G.Z. Cheng, Int. J. Hydrogen Energy 39 (2014) 4947–4953.
[15] Z.L. Wang, J.M. Yan, Y. Ping, H.L. Wang, W.T. Zheng, Q. Jiang, Angew. Chem. Int. Ed. 52 (2013) 4406–4409.
[16] Z.L. Wang, Y. Ping, J.M. Yan, H.L. Wang, Q. Jiang, Int. J. Hydrogen Energy 39 (2014) 4850–4856.
[17] Q.L. Zhu, N. Tsumori, Q. Xu, Chem. Sci. 5 (2014) 195–199.
[18] K. Jiang, K. Xu, S.H. Zou, W.B. Cai, J. Am. Chem. Soc. 136 (2014) 4861–4864.
[19] J. Wang, X.B. Zhang, Z.L. Wang, L.M. Wang, Y. Zhang, Energy Environ. Sci. 5 (2012) 6885–6888.
[20] Y.L. Qin, J. Wang, F.Z. Meng, L.M. Wang, X.B. Zhang, Chem. Commun. 49 (2013) 10028–10030.
[21] K. Jiang, W.B. Cai, Appl. Catal. B 147 (2014) 185–192.
[22] N.F. Zheng, J. Fan, G.D. Stucky, J. Am. Chem. Soc. 128 (2006) 6550–6551.
[23] B.K. Suresh, S. Udishnu, J. Balaji, ChemSusChem 4 (2011) 317–324.
[24] C. Du, Y.X. Liao, X. Hua, W. Luo, S.L. Chen, G.Z. Cheng, Chem. Commun. 50 (2014) 12843–12846.